The Astrophysical Journal Letters, 921:L42 (7pp), 2021 November 10 https://doi.org/10.3847/2041-8213/ac341f

A Kiloparsec-scale Molecular Wave in the Inner Galaxy: Feather of the Milky Way?

V. S. Veena[1], P. Schilke[1], Á. Sánchez-Monge[1], M. C. Sormani[2], R. S. Klessen[2], F. Schuller[3], D. Colombo[4], T. Csengeri[5], M. Mattern[6], and J. S. Urquhart[7]
[1] I. Physikalisches Institut, Universität zu Köln, Zülpicher Str.77, D-50937 Köln, Germany; veena@ph1.uni-koeln.de
[2] Institut für Theoretische Astrophysik, Zentrum für Astronomie, Universität Heidelberg, Albert-Ueberle-Str 2, D-69120 Heidelberg, Germany
[3] Leibniz-Institut für Astrophysik Potsdam (AIP), An der Sternwarte 16, D-14482 Potsdam, Germany
[4] Max-Planck-Institut für Radioastronomie, auf dem Hügel 69, D-53121 Bonn, Germany
[5] Laboratoire d'Astrophysique de Bordeaux, Univ. Bordeaux, CNRS, B18N, alléé Geoffroy Saint-Hilaire, F-33615 Pessac, France
[6] Laboratoire d'Astrophysique (AIM), CEA, CNRS, Université Paris-Saclay, Université Paris Diderot, Sorbonne Paris Cité, F-91191 Gif-sur-Yvette, France
[7] Centre for Astrophysics and Planetary Science, University of Kent, Canterbury CT2 7NH, UK
Received 2021 July 22; revised 2021 October 20; accepted 2021 October 26; published 2021 November 11

Abstract

We report the discovery of a velocity coherent, kiloparsec-scale molecular structure toward the Galactic center region with an angular extent of 30° and an aspect ratio of 60:1. The kinematic distance of the CO structure ranges between 4.4 and 6.5 kpc. Analysis of the velocity data and comparison with the existing spiral arm models support that a major portion of this structure is either a subbranch of the Norma arm or an interarm giant molecular filament, likely to be a kiloparsec-scale feather (or spur) of the Milky Way, similar to those observed in nearby spiral galaxies. The filamentary cloud is at least 2.0 kpc in extent, considering the uncertainties in the kinematic distances, and it could be as long as 4 kpc. The vertical distribution of this highly elongated structure reveals a pattern similar to that of a sinusoidal wave. The exact mechanisms responsible for the origin of such a kiloparsec-scale filament and its wavy morphology remains unclear. The distinct wave-like shape and its peculiar orientation makes this cloud, named as the Gangotri wave, one of the largest and most intriguing structures identified in the Milky Way.

Unified Astronomy Thesaurus concepts: Milky Way Galaxy (1054); Galaxy kinematics (602); Galaxy structure (622); Interstellar medium (847); Giant molecular clouds (653); Submillimeter astronomy (1647)

1. Introduction

Characterizing the large-scale spiral structure of the Milky Way remains a challenge since the solar system lies within the Galaxy. Most Milky Way models suggest the presence of a central bar besides four major gaseous spiral arms and some extra arm segments and spurs (Reid et al. 2019). This is derived from the velocity data obtained from the distribution of atomic, molecular, and ionized hydrogen and the CO molecule as well as parallax information from stellar sources within the Milky Way (e.g., Oort et al. 1958; Georgelin & Georgelin 1976; Dame et al. 2001; Gaia Collaboration et al. 2018). The observational studies of external spiral galaxies reveal that spiral arms are not smooth and continuous features. Instead, they mostly comprise multiple substructures that are referred to as spurs, branches, or feathers, and which give the arms their clumpy or patchy appearance (Lynds 1970; Weaver 1970; Elmegreen 1985; La Vigne et al. 2006; Schinnerer et al. 2017).

With the advent of sensitive and high-resolution infrared and millimeter surveys, there has been tremendous progress in unveiling the intricate morphology of the large-scale gas structures in our Galaxy. For example, the identification of multiple giant molecular filaments (GMFs) on scales of hundreds of parsecs has redefined our view of the Milky Way's structural dynamics (e.g., Jackson et al. 2010; Ragan et al. 2014; Wang et al. 2015; Abreu-Vicente et al. 2016; Zucker et al. 2018). Few of these extremely long and narrow GMFs appear to lie parallel to and within few parsecs from the Galactic midplane. Their line-of-sight velocities suggest that GMFs are often associated with nearby spiral arms. They are frequently called "bones/spines," and trace the densest regions of the Galactic spiral arms. Hence, they could potentially be used to map the skeleton of our Galaxy (e.g., Goodman et al. 2014). In an alternate scenario, they could be "spurs/feathers" emanating from spiral arms or interarm clouds similar to those in simulations or observed in nearby galaxies (e.g., Colombo et al. 2014; Ragan et al. 2014; Duarte-Cabral & Dobbs 2017; Smith et al. 2020).

In this work, we report the discovery of a highly unusual filamentary cloud located within 5 kpc of the Galactic center region ($325° < l < 355°$). The extreme length, sinusoidal wave-like morphology, and relative orientation with respect to the adjacent Norma and 3 kpc spiral arms make this structure one of the most unusual features identified in the Milky Way. Given the uniqueness of this molecular structure, we name it as "Gangotri wave," after the Gangotri glacier, the primary source of the Ganges, which is the longest river in India. The observations, data analysis, and results are presented in Sections 2 and 3, respectively, and discussed in detail in Section 4. Finally, we present our conclusions in Section 5.

2. Data

2.1. SEDIGISM

The Structure, Excitation, and Dynamics of the Inner Galactic Interstellar Medium (SEDIGISM) project is a CO survey covering 78 deg^2 of the inner Galaxy ($-60° < l < +18°$, $|b| < 0.5°$) in the $J = 2$–1 rotational transition of ^{13}CO and C^{18}O (Schuller et al. 2017, 2021; Duarte-Cabral et al. 2021; Urquhart et al. 2021). The ^{13}CO isotopologue of CO is less abundant than ^{12}CO by factors up to 100, making it an ideal tracer of the cold and dense

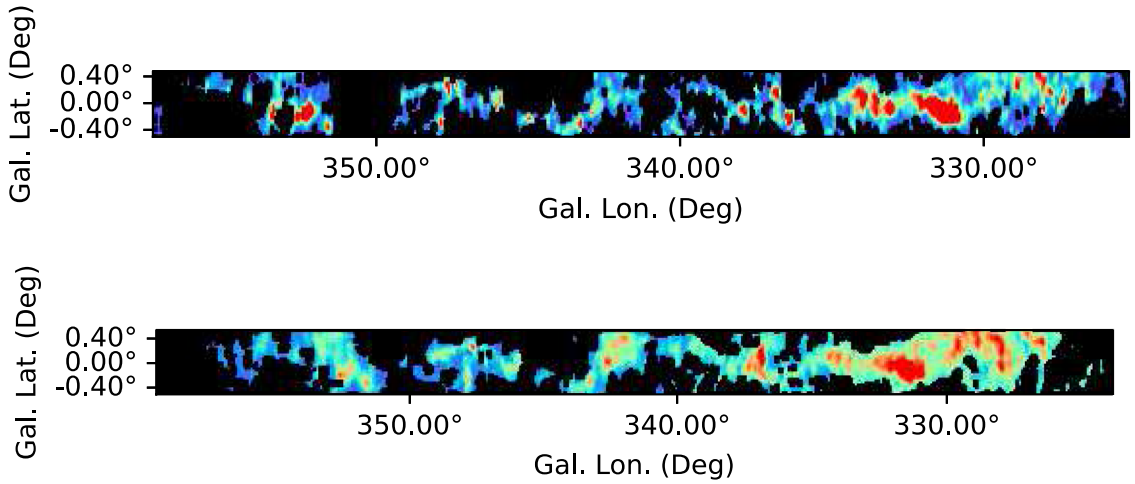

Figure 1. (Top) ^{13}CO integrated intensity map from the SEDIGISM survey in the velocity range −95 to −75 km s^{-1} showing a wave-like feature. (Bottom) ^{12}CO integrated intensity map from the ThrUMMS survey in the same velocity range as the top panel, smoothed to an angular resolution of 5′. Images are stretched along the *y*-axis for a better visualization.

molecular clouds of the Milky Way. The entire 78 deg^2 survey area is divided into 2.0 × 1.0 deg^2 fields. The spatial and spectral resolutions are 28″ and 0.25 km s^{-1}, respectively, and the typical rms noise in each field is ∼0.8 K. In order to search for potential giant filaments in the inner Galaxy, we have combined all the individual tiles to produce 78 deg^2 mosaic maps of ^{13}CO and C^{18}O emission. For this, we have first smoothed the individual tiles to a lower velocity resolution of 1.5 km s^{-1}. We then combined the smoothed tiles to create a single mosaic using the Montage software (Berriman et al. 2003). In this Letter, we have used a spatially smoothed mosaic with an angular resolution of 5′ for a better visualization of the features.

2.2. ThrUMMS

The Three-mm Ultimate Mopra Milky Way Survey (ThrUMMS; Barnes et al. 2015) is the millimeter-wave molecular-line mapping survey that covers 60° × 2° of the fourth quadrant of the Galaxy in the $J = 1$–0 rotational transition of ^{12}CO, ^{13}CO, C^{18}O, and CN at spatial and spectral resolutions of 1′ and 0.3 km s^{-1}, respectively. We have used the ^{12}CO data tiles to create a mosaic for our analysis.

2.3. SGPS

The Southern Galactic Plane Survey (SGPS; McClure-Griffiths et al. 2005) is a H I survey combining data from the Australia Telescope Compact Array and the Parkes Radio Telescope covering 325 deg^2 at arcminute resolution. We have used the SGPS I data tiles with an angular resolution of 2.′2 and spectral resolution of 0.8 km s^{-1}.

3. Results

In order to search for potential bones/spurs in the CO emission, we have used the ^{13}CO mosaic from the SEDIGISM survey. Integrated intensity maps were generated at velocity intervals of 10 km s^{-1}. The resultant maps were visually inspected to identify filamentary features. Figure 1 (top) shows the ^{13}CO integrated intensity map of the region from $325° < l < 358°$ in the velocity range −95 km s^{-1} to −75 km s^{-1}. The map reveals an emission feature that is extending up to 30° in longitude from $325° < l < 355°$. The ratio of angular length (30°) to angular width (∼0.5°) implies a projected aspect ratio of 60:1. This illustrates the highly elongated/filamentary morphology of the feature, which is also evident in the ^{12}CO integrated map (Figure 1, bottom) obtained from ThrUMMS. The SEDIGISM ^{13}CO channel maps toward the region are presented in Figure A1 of the Appendix.

3.1. Distance and Size of the Filament

There are no previous distance estimates of the filament available in the literature. As there are no trigonometric parallaxes, it is difficult to obtain accurate values. However, an approximate distance can be obtained using the kinematic method (e.g., Roman-Duval et al. 2009). For this, the velocity distribution of the ^{13}CO emission can be used. In order to obtain the velocity distribution toward the filament, we availed the fully automated Gaussian decomposer `GAUSSPY+` (Lindner et al. 2015; Riener et al. 2019). It makes use of the `GAUSSPY` algorithm to analyze the complex spectra extracted from the Galactic plane by decomposing them into multiple Gaussian components. For the spectral decomposition, we subdivided the 30° mosaic into submosaics of sizes of 5° each. We have taken the default parameters for the decomposition provided by Riener et al. (2019), except for the smoothing parameters α_1 and α_2. To determine these parameters, we generated the training sets that were used to train `GAUSSPY+` with 1000 randomly selected spectra from CO subcubes with sizes of 5° each. The decomposition of the entire 30° mosaic resulted in 13.2×10^6 Gaussian components. Since the filamentary structure is mainly identified in the velocity range [−95, −75] km s^{-1}, we excluded all the components outside this specified velocity range from further analysis.

As the filament is located inside the solar circle, the distance calculations are hampered by the kinematic distance ambiguity (KDA). For each radial velocity along a given line of sight, there are two possible values, one corresponding to the near distance and the other to the far distance. In order to resolve the KDA, the Hi-GAL compact source catalog (Elia et al. 2017) is used. Only sources with LSR velocity matching that of the wavy filament and having a reliable distance estimate are selected for the analysis. According to Elia et al. (2017), these reliable values are determined by first estimating the kinematic distance to the sources using the CO data and the Galactic rotation curve model of Brand & Blitz (1993). Then, the KDA is resolved by matching positions with a catalog of sources

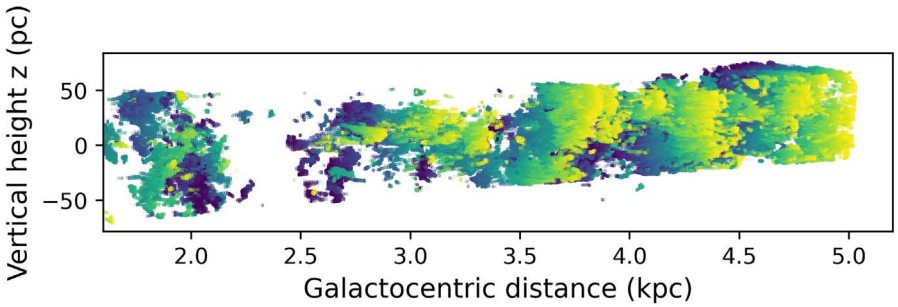

Figure 2. Galactocentric distance versus vertical distance from the Galactic plane (z) of the cloud in the velocity range [−95, −75] km s^{-1} showing the vertical oscillations with respect to the Galactic midplane.

with known distances (such as H II regions and masers) or, alternatively, with features in extinction maps. The distribution of Hi-GAL sources correlate well with that of the filament (see Figure 1). The distances of the Hi-GAL sources fall in the range 4.5–7.0 kpc, favoring the near distance for the filament. In addition to this, the infrared star count and extinction map toward the fourth quadrant of the Galaxy (Soto et al. 2019) are also utilized to resolve the KDA. These maps show that there is relatively lower stellar density and higher dust extinction toward the region corresponding to the position of the filament. This again implies that the filament is likely to be located at the near side.

The heliocentric distance to the filament at $l \sim 325°$ is ∼4.5 kpc, whereas it extends farther away, toward the Galactic center region (distance >7 kpc) at higher longitudes. Since there are large uncertainties involved in the kinematic distance estimates beyond $l \sim 350°$, getting accurate distance distribution of the filament is highly challenging. Using the derived kinematic distances, the deprojected length of the GMF is estimated to be 4 kpc. Assuming that the distance to the filament is 4.4 kpc, we get a lower limit to the spatial extent of the filament of 2.4 kpc. The average vertical width of the filament is under 50 pc, resulting in an aspect ratio of 60:1.

3.2. Morphology and the Three-dimensional Orientation of the Filament

Apart from its velocity coherent distribution at kiloparsec scales, the GMF also exhibits an intriguing two-dimensional projected morphology. The visual inspection of the integrated intensity map shows a sinusoidal wave-like pattern with corrugations in the Galactic latitude along the GMF. The undulations appear to be dampening toward the right-hand side ($l < 335°$) of the GMF similar to that of the recently discovered Radcliffe wave (Alves et al. 2020, see Section 4.2.2). Figure 2 shows the distribution of the GMF with respect to the plane of the Milky Way. The vertical oscillations span ∼±70 pc in the Galactic midplane. These oscillations are within the average thickness of the molecular disk of the Milky Way (∼160 pc; e.g., Nakanishi & Sofue 2006). Assuming the lower limit distance of 4.5 kpc, the wavelength (toward the left side of the GMF, i.e., $l \sim 350°$) is estimated to be 600 pc. There appears to be a break in the wave at $l \sim 350°$ in the ^{13}CO map that is less prominent in the ^{12}CO intensity map that could be due to lack of high-density molecular gas in the region, possibly from star formation activity in the past. The wave is relatively narrower toward the east (i.e., $l > 345°$). Toward the west, where the velocities are consistent with the Norma arm, the emission is more diffuse in nature. This could also be due to the foreground or background contamination from other molecular clouds along the Norma arm. There are numerous H II regions, dense cores, and infrared bubbles (e.g., MWP1G352880-002000S; Simpson et al. 2012) located along the filament indicating the star formation flurry of the cloud. The wavy structure is not evident in the submillimeter continuum map (see Figure A2 in the Appendix) due to possible contamination from molecular clouds in the foreground and background.

3.3. Column Density and Mass

The total column density of the wavy filament is estimated using the standard method described in earlier studies (e.g., Carlhoff et al. 2013). In order to estimate the column density of the filament, we have converted the integrated intensity of ^{13}CO(2–1) emission into H_2 column density using a mean conversion factor, $X_{\mathrm{CO(2-1)}}^{13} = 1.08 \times 10^{21}$ cm^{-2} (K km s^{-1})$^{-1}$ adopted from Schuller et al. (2017). A column density map of the filament has been obtained. From the map, the peak and mean column densities along the filament are estimated as 2.1×10^{23} cm^{-2} and 6.1×10^{21} cm^{-2}, respectively.

The total column density of the filament can be converted directly to the mass of the filament using the expression

$$M = N(\mathrm{H_2})\,\mu m_{\mathrm{H}} A. \quad (1)$$

Here M represents the mass of the filament, A is the area of the filament, μ is the mean weight of the molecular gas taken to be 2.86 assuming that the gas is 70% molecular hydrogen by mass (Ward-Thompson et al. 2010), and m_{H} is the mass of the hydrogen atom. Using this equation, we find the total mass of the cloud as $8.7 \times 10^6\,M_{\odot}$. We point out that this is a lower limit as we estimated the mass assuming a lower limit distance to the filament that is 4.5 kpc.

3.4. Velocity Structure of the Filament and Location in the Galaxy

The Galactic longitude versus LSR velocity (l,V) diagram can be used to understand the velocity structure of the wavy filament and its approximate location within the Milky Way. Figure 3 (left) shows the distribution of the wavy filament over the Galactic CO emission. Overplotted are the spiral arm models of Reid et al. (2016). From the figure, it is evident that in the longitude range below 343°, the emission matches well with the model of Norma spiral arm. In the longitude range 343°–350°, the velocity of the structure deviates from the Norma arm with maximum deviated velocity of ∼35 km s^{-1}. Beyond 350° longitude, the emission matches quite well with that of the 3 kpc spiral arm model. The break in the wavy structure observed in the integration emission maps is also seen in the (l,V) diagram. A possible explanation is that the wavy

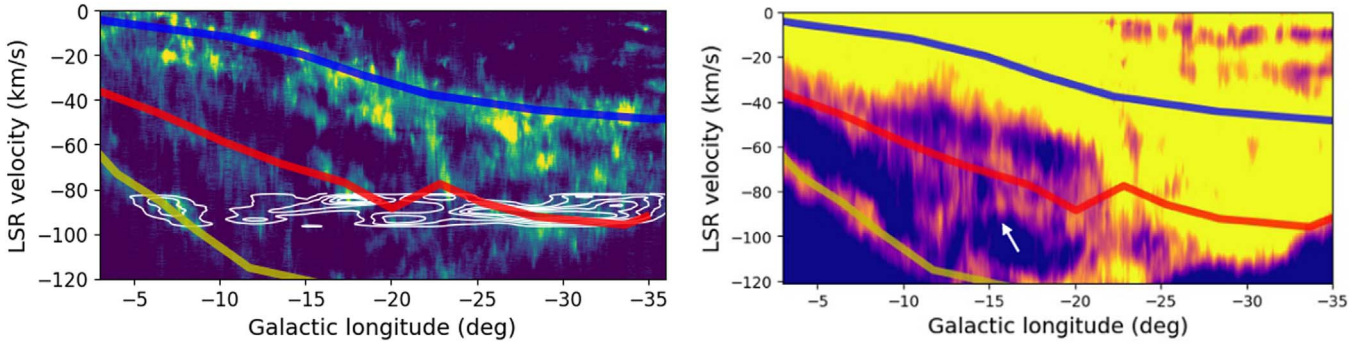

Figure 3. (Left) ^{12}CO emission from ThrUMMS as a function of LSR velocity and Galactic longitude. The colored lines (blue: Scutum–Centaurus arm, red: Norma arm, yellow: 3 kpc arm) correspond to the spiral arm models of Reid et al. (2016). Overplotted are the ^{12}CO contours corresponding to the Gangotri wave. (Right) H I emission from the SGPS survey as a function of LSR velocity and Galactic longitude overlaid with the spiral arm models of Reid et al. (2016). The Gangotri wave is seen as a distinct structure branching out from the main Norma spiral arm emission, pointed to with an arrow.

filament is not a coherent structure and rather a superposition of features from Norma and 3 kpc arms. In order to investigate this further, we have also generated a H I (l,V) diagram using SGPS data. Since H I traces low-density gas compared to CO, any connection should be prominent in the H I plot. Figure 3 (right) shows the H I (l,V) diagram. In the plot, the emission corresponding to the wavy structure appears very prominent in the Norma–3 kpc interarm region. The structure appears to be branching out from the main Norma arm at longitudes beyond 340° extending further toward the direction of 3 kpc arm. This implies that the structure is not entirely confined to the Norma arm. The structure is 2 kpc in extent, excluding emission from the 3 kpc region. Even though the emission corresponding to the 3 kpc arm at present appears to be disconnected from the structure connected to the Norma arm, the vertical oscillation seems to transcend this gap. Either the connection existed in the past, or the cause for the vertical oscillation does not require a physical connection of the gaseous structures, which would be the case, for example, with waves in the gravitational potential. The velocity distribution of the entire structure also shows fluctuations along the Galactic longitude, evident in the (l,V) diagrams. Such large-scale velocity fluctuations and oscillatory gas flows are detected in molecular clouds toward the Galactic and extragalactic environments that may form via gravitational instabilities (Henshaw et al. 2020).

4. Discussion

4.1. Orientation of the GMF with Respect to the Spiral Arms

In order to better understand the physical origin of this molecular wavy structure, an investigation on its large-scale distribution with respect to the spiral arms of the Galaxy is required. The most important question is whether the cloud belongs to a spiral arm or it is an interarm spur. It is seen from Section 3.4 that the (l,V) distribution of the wavy structure is not consistent with one particular spiral arm. Using the kinematic distance estimates in Section 3.4 and the corresponding Galactic longitudes combined with the spiral arm models of Reid et al. (2019), a planar view of the distribution of wavy filament with respect to the spiral arms of the Milky Way can be determined, as indicated in Figure 4. The major fraction of the structure on the near side appears to be within the Norma arm. However, it extends farther out into the interarm region. This means that the filament being a bone/spine can be ruled out, as such features, per definition, are closely associated with the spiral arms (Goodman et al. 2014). At the distance range

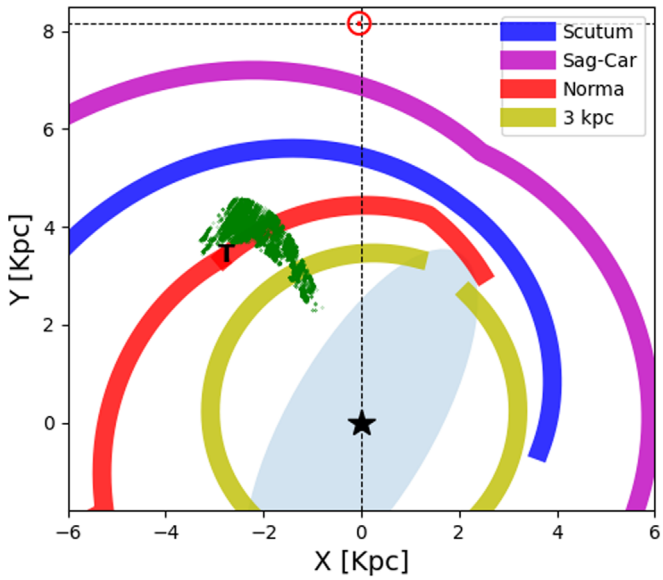

Figure 4. Distribution of the GMF with respect to the spiral arm models of Reid et al. (2019). The location of the Norma arm tangent point is also marked.

corresponding to the Gangotri wave, the typical spiral arm width is estimated around 100–250 pc (Reid et al. 2019). If we exclude the emission matching with Norma and 3 kpc arms, the filament is extending over 500 pc in the interarm region (assuming a minimum heliocentric distance of 4.5 kpc). Kuhn et al. (2021) recently identified a 1 kpc, high pitch angle and high aspect ratio (7:1) structure associated with the Sagittarius arm. This feature is believed to be either an isolated entity, a substructure within the spiral arm, or an interarm spur. In case of the Gangotri wave, although the connection with 3 kpc arm is not firm, the observed orientation suggests that the structure is either a subarm/branch of the Norma arm or an interarm spur, similar to those observed in external spiral galaxies.

We have also used the numerical models to analyze the impact of noncircular motions induced by the bar near the Galactic center on the orientation and distance of the Gangotri wave (e.g., Fux 1999). Figure 5 shows the orientation and distance of the based on the hydrodynamical simulations of Sormani et al. (2018). The model includes a rigidly rotating barred spiral potential fitted to the Milky Way and allows us to account for the errors in kinematic distances due to the noncircular motions driven by the bar. From the plots, it is

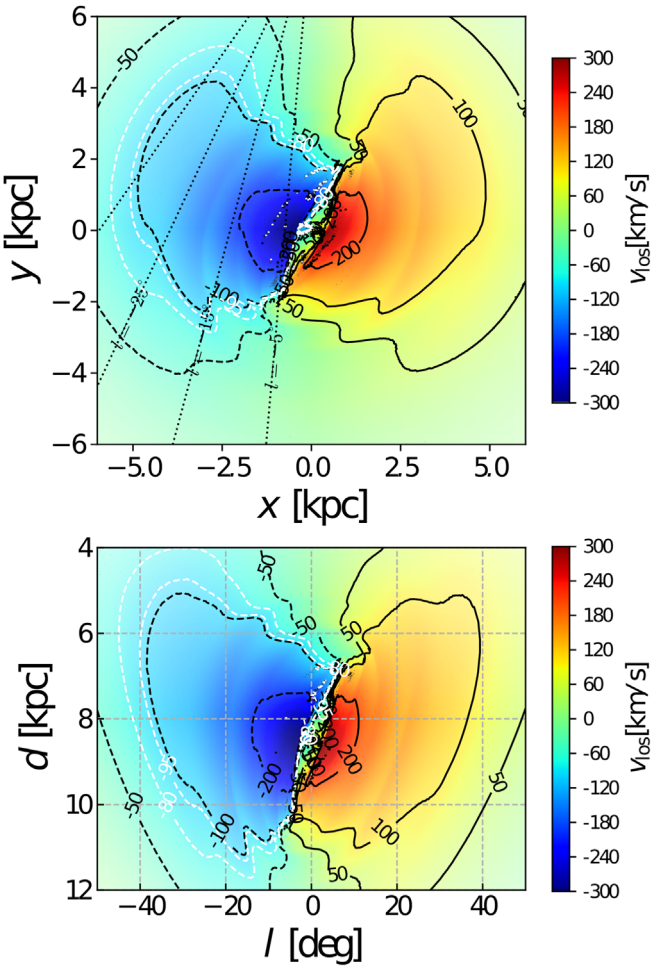

Figure 5. Mass-averaged line-of-sight velocity in the (x, y) plane (top) and (l, d) plot (bottom) for a snapshot of the simulations in Sormani et al. (2018). The snapshot is similar to those shown in Figures 8, 9, and 10 in their paper. The labeled contours indicate the line-of-sight velocities. The white dashed contours represent velocities of −80 and −95 km s^{-1}, corresponding to those of the Gangotri wave, according to the model. Here, l and d correspond to Galactic longitude and distance from the Sun, and (x, y) corresponds to Galactocentric coordinates, respectively.

evident that the kinematic distance of the Gangotri wave, after correcting for the noncircular motions lies in the range ∼4.0–6.5 kpc. Thus, this confirms the subarm/interarm nature of the wave.

Weaver (1970) noted that many of the nearby spiral galaxies have spurs that appear to originate on the outside of a spiral arm and extend into the interarm regions. Strong dust lanes along the inner edge of the arms identified in some of the spiral galaxies are often termed as feathers (Lynds 1970; Piddington 1973). A Hubble Space Telescope survey by La Vigne et al. (2006) discovered feathers toward 45 spiral galaxies. They have concluded that the feathers are common in prototypical Sc galaxies as well as in Sb galaxies. The typical feathers are described as dark, delineated extinction features, that emerge from primary dust lanes (PDLs) that run along the inside part of the arm and then extend well into the interarm regions. Some of these feathers are several kiloparsecs in extent and appear to merge with the PDL of the next arm (e.g., Figures 1 and 2 of La Vigne et al. 2006). As the Milky Way is a barred spiral galaxy, we expect it to have such interarm feathers as well. Thus, the newly identified Gangotri wave could be a potential feather of the Milky Way.

4.2. Physical Origin of the Gangotri Wave

4.2.1. Interarm Nature: Galactic Feather?

From Section 4.1, it is clear that the Gangotri wave is a kiloparsec-scale Norma subarm or interarm spur possibly connecting the near side of the Norma and 3 kpc spiral arms. The formation of such spiral arm substructures, such as feathers and spurs in global magnetohydrodynamic (MHD) simulations, has been explored in detail in many works (e.g., Kim & Ostriker 2002; Shetty & Ostriker 2006). There is still no consensus on the mechanism that generates these substructures. Proposals include self-gravity, magneto-Jeans instabilities, the wiggle instability, shear due to differential rotation, and the effect of correlated supernova (SN) feedbacks.

The self-gravity and magnetic fields within the spiral arms lead to the rapid growth of overdensities. The differential compression of gas flowing through such arms could then result in the formation of sheared structures in the interarm regions. Simulations of GMFs in spiral galaxies have furthermore demonstrated that GMFs can be formed from gas clouds that exit a spiral arm and get stretched by the differential rotation of the gas (Smith et al. 2014; Duarte-Cabral & Dobbs 2017). These GMFs can span lengths >500 pc in H_2. However, CO is seen to be present only on the denser regions of the clouds, putting an upper limit on length of CO filaments as ∼100 pc.

The wiggle instability (WI) of spiral shocks in a galactic disk has been proposed as the mechanism responsible for the formation of gaseous feathers in spiral galaxies. According to Wada & Koda (2004), the WI is a manifestation of Kelvin–Helmholtz (KH) instability of the shear layer behind the shock. This view has been challenged by later works, where the WI is proven to be distinct from the KH instability (Kim et al. 2014; Sormani et al. 2017). 3D interstellar medium (ISM) simulations including the effects of star formation and SN feedbacks (TIGRESS) by Kim et al. (2020) have shown that the correlated SN feedback produces short-lived spurs/feathers ($t \sim 30$ Myr) with magnetic fields parallel to their length, in contrast to long-lived features ($t \sim 200$ Myr) with perpendicular magnetic fields induced by gravitational instabilities. Magnetic field observations of the spur/feather could therefore be used to find vital clues regarding whether the structure is produced by magneto-Jeans instability or SN feedbacks. It is possible that the feather-like nature of the Gangotri wave is due to a combination of all of the above mechanisms.

4.2.2. Wavy Morphology

Apart from its kiloparsec-scale extent and the interarm nature, another intriguing feature of the Gangotri wave is its sinusoidal wave-like morphology. Small-scale bending waves are detected in the dust lanes of five nearby edge-on galaxies (Narayan et al. 2020). The corrugation amplitude is found in the range of 70–200 pc with the corresponding wavelengths in the range 1–5 kpc. These corrugations are seen in stars, gas, and dust, indicating that they are most likely to be caused by gravitational instabilities.

A sine wave-like structure perpendicular to the plane is observed in the vertical profile of the Carina–Sagittarius spiral arm ($-70^\circ \leqslant l \leqslant 30^\circ$) obtained from the young open cluster distribution (Alfaro et al. 1992). The wavelength of the structure is ∼2.4 kpc, which is similar to the distribution of atomic hydrogen in the same spiral segment. Three-dimensional density waves are

envisaged as the likely mechanism responsible for the observed vertical structure. Alves et al. (2020) identified a narrow and coherent 2.7 kpc structure in the solar neighborhood. The structure, known as the Radcliffe wave, contains many of the clouds thought to be associated with the Gould belt. The 3D distribution of the Radcliffe wave is described by a damped sinusoidal wave with an average period of 2 kpc and maximum amplitude of 60 pc. The most plausible hypothesis regarding the origin of the Radcliffe wave is that it is the outcome of a large-scale Galactic process of gas accumulation either from a shock front in a spiral arm or from gravitational settling and cooling on the plane of the Milky Way.

An analysis of the 3D distribution of massive stars based on Alma and Gaia DR2 catalogs in the solar neighborhood by Pantaleoni González et al. (2021) discovered a corrugation pattern, the Cepheus spur, extending from Orion–Cygnus arm toward the Perseus arm, which is likely associated with the Radcliffe wave. Wave-like signatures in the distribution of stars in both density and velocity space have been observed in different regions of the Milky Way where models proposed that the perturbations are caused by the interaction of a satellite galaxy with the disk of the Milky Way (e.g., Binney & Schönrich 2018). Another theory is that the vertical perturbations can be due to a dynamical coupling between the Galactic bar and the spiral arms (e.g., Monari et al. 2016). The Gangotri wave is distinct from previously discovered Galactic corrugations in that it is the first velocity coherent dense gas filament exhibiting vertical corrugations. With the current data, it is difficult to pinpoint the exact mechanism responsible for the origin of the Gangotri wave.

5. Conclusions

We have identified a new velocity coherent filamentary structure in the fourth Galactic quadrant at $325° < l < 355°$, which we call the Gangotri wave. The structure has a spatial extent of at least 2.0 kpc with a high aspect ratio (60:1) and is morphologically similar to a sinusoidal wave. A lower limit to the total mass of the Gangotri wave is estimated as $8.7 \times 10^6\ M_\odot$. Part of the velocity of the structure is consistent with that of the Norma arm toward one end, whereas it corresponds to the velocity profile of the 3 kpc arm toward the other end. The overall velocity structure is consistent with that expected for a spiral subarm or an interarm feather, similar to those observed in external spiral galaxies. Density waves, MHD instabilities, interaction of the Galactic bar with the spiral arms, as well as interaction of external dwarf galaxies with the Milky Way in the past have been suggested as likely scenarios responsible for the formation of such an enigmatic structure. With the present data, however, we cannot conclusively identify its physical origin.

The authors thank the referee for the comments and suggestions, that improved the quality of the Letter. We thank Zhi Li for providing the spiral arm data based on the (l, v) model of Reid et al. (2016). This research made use of Montage which is funded by the National Science Foundation under grant No. ACI-1440620, and was previously funded by the National Aeronautics and Space Administration's Earth Science Technology Office, Computation Technologies Project, under Cooperative Agreement Number NCC5-626 between NASA and the California Institute of Technology. V.V.S. acknowledges support from the Alexander von Humboldt Foundation.

Appendix

13CO channel maps and cold dust emission map of the Gangotri wave is presented in the Appendix.

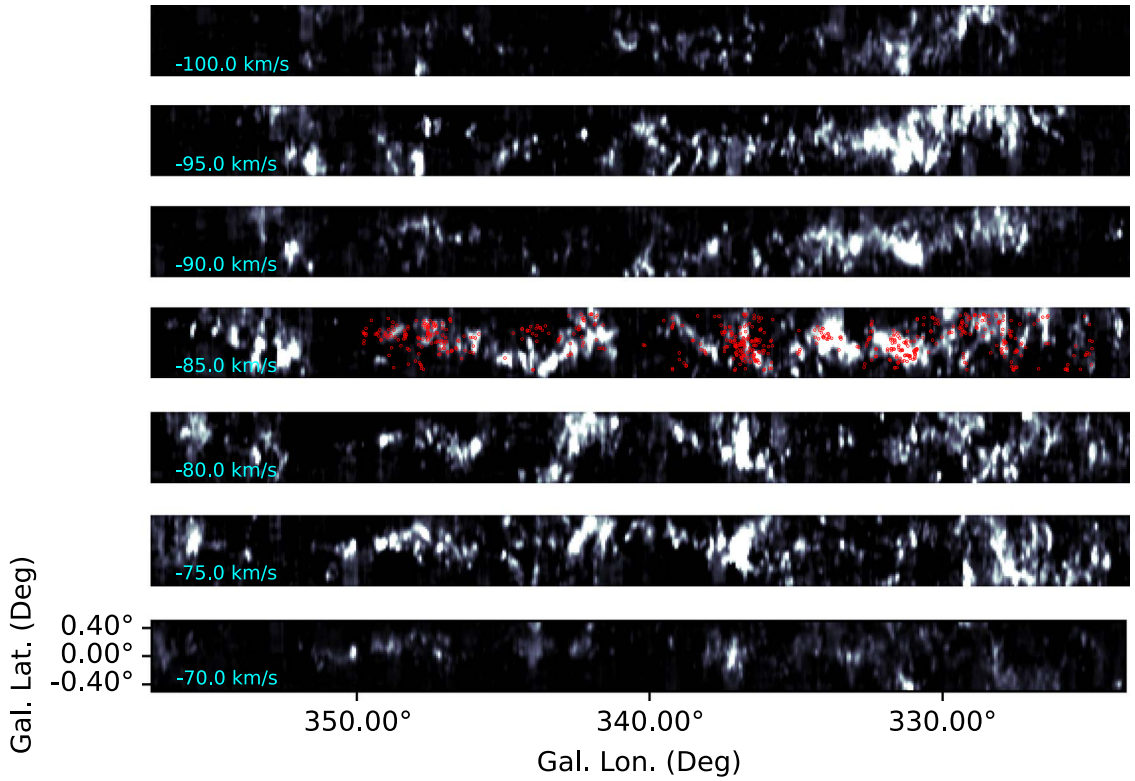

Figure A1. ^{13}CO channel maps of the Gangotri wave in the velocity range $V = [-100\ \mathrm{km\ s^{-1}}, -70\ \mathrm{km\ s^{-1}}]$. Overlaid on the $V = -85\ \mathrm{km\ s^{-1}}$ channel map are the Hi-GAL sources with reliable distance estimates (red).

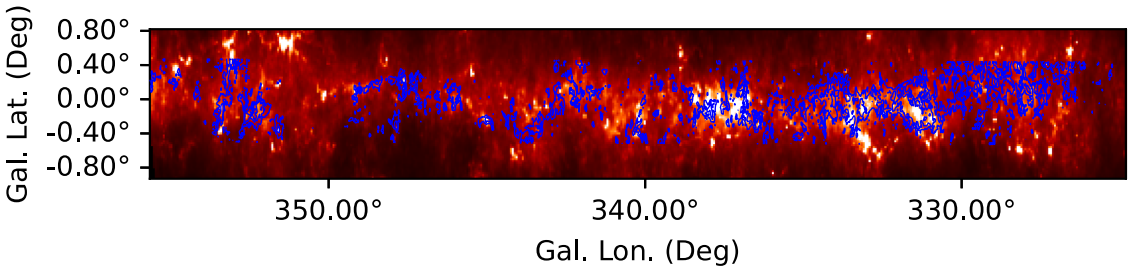

Figure A2. Dust continuum map from Herschel at 500 μm overlaid with ^{13}CO integrated intensity contours. The contour levels are 150 K km s^{-1} and 450 K km s^{-1}. The image is stretched along the y-axis for better visualization.

ORCID iDs

V. S. Veena https://orcid.org/0000-0002-0801-8550
P. Schilke https://orcid.org/0000-0003-2141-5689
Á. Sánchez-Monge https://orcid.org/0000-0002-3078-9482
M. C. Sormani https://orcid.org/0000-0001-6113-6241
R. S. Klessen https://orcid.org/0000-0002-0560-3172
T. Csengeri https://orcid.org/0000-0002-6018-1371

References

Abreu-Vicente, J., Ragan, S., Kainulainen, J., et al. 2016, A&A, 590, A131
Alfaro, E. J., Cabrera-Cano, J., & Delgado, A. J. 1992, ApJ, 399, 576
Alves, J., Zucker, C., Goodman, A. A., et al. 2020, Natur, 578, 237
Barnes, P. J., Muller, E., Indermuehle, B., et al. 2015, ApJ, 812, 6
Berriman, G. B., Good, J. C., Curkendall, D. W., et al. 2003, in ASP Conf. Ser., 295, Astronomical Data Analysis Software and Systems XII, ed. H. E. Payne, R. I. Jedrzejewski, & R. N. Hook (San Francisco, CA: ASP), 343
Binney, J., & Schönrich, R. 2018, MNRAS, 481, 1501
Brand, J., & Blitz, L. 1993, A&A, 275, 67
Carlhoff, P., Nguyen Luong, Q., Schilke, P., et al. 2013, A&A, 560, A24
Colombo, D., Hughes, A., Schinnerer, E., et al. 2014, ApJ, 784, 3
Dame, T. M., Hartmann, D., & Thaddeus, P. 2001, ApJ, 547, 792
Duarte-Cabral, A., Colombo, D., Urquhart, J. S., et al. 2021, MNRAS, 500, 3027
Duarte-Cabral, A., & Dobbs, C. L. 2017, MNRAS, 470, 4261
Elia, D., Molinari, S., Schisano, E., et al. 2017, MNRAS, 471, 100
Elmegreen, D. M. 1985, in The Milky Way Galaxy, ed. H. vanWoerden, R. J. Allen, & W. B. Burton (Dordrecht: Reidel), 255
Fux, R. 1999, A&A, 345, 787
Gaia Collaboration, Katz, D., Antoja, T., et al. 2018, A&A, 616, A11
Georgelin, Y. M., & Georgelin, Y. P. 1976, A&A, 49, 57
Goodman, A. A., Alves, J., Beaumont, C. N., et al. 2014, ApJ, 797, 53
Henshaw, J. D., Kruijssen, J. M. D., Longmore, S. N., et al. 2020, NatAs, 4, 1064
Jackson, J. M., Finn, S. C., Chambers, E. T., Rathborne, J. M., & Simon, R. 2010, ApJL, 719, L185
Kim, W.-T., Kim, C.-G., & Ostriker, E. C. 2020, ApJ, 898, 35
Kim, W.-T., Kim, Y., & Kim, J.-G. 2014, ApJ, 789, 68
Kim, W.-T., & Ostriker, E. C. 2002, ApJ, 570, 132
Kuhn, M. A., Benjamin, R. A., Zucker, C., et al. 2021, A&A, 651, L10
La Vigne, M. A., Vogel, S. N., & Ostriker, E. C. 2006, ApJ, 650, 818
Lindner, R. R., Vera-Ciro, C., Murray, C. E., et al. 2015, AJ, 149, 138
Lynds, B. T. 1970, The Spiral Structure of our Galaxy, ed. W. Becker & G. I. Kontopoulos, 26
McClure-Griffiths, N. M., Dickey, J. M., Gaensler, B. M., et al. 2005, ApJS, 158, 178
Monari, G., Famaey, B., Siebert, A., et al. 2016, MNRAS, 461, 3835
Nakanishi, H., & Sofue, Y. 2006, PASJ, 58, 847
Narayan, C. A., Dettmar, R.-J., & Saha, K. 2020, MNRAS, 495, 3705
Oort, J. H., Kerr, F. J., & Westerhout, G. 1958, MNRAS, 118, 379
Pantaleoni González, M., Maíz Apellániz, J., Barbá, R. H., & Reed, B. C. 2021, MNRAS, 504, 2968
Piddington, J. H. 1973, ApJ, 179, 755
Ragan, S. E., Henning, T., Tackenberg, J., et al. 2014, A&A, 568, A73
Reid, M. J., Dame, T. M., Menten, K. M., & Brunthaler, A. 2016, ApJ, 823, 77
Reid, M. J., Menten, K. M., Brunthaler, A., et al. 2019, ApJ, 885, 131
Riener, M., Kainulainen, J., Henshaw, J. D., et al. 2019, A&A, 628, A78
Roman-Duval, J., Jackson, J. M., Heyer, M., et al. 2009, ApJ, 699, 1153
Schinnerer, E., Meidt, S. E., Colombo, D., et al. 2017, ApJ, 836, 62
Schuller, F., Csengeri, T., Urquhart, J. S., et al. 2017, A&A, 601, A124
Schuller, F., Urquhart, J. S., Csengeri, T., et al. 2021, MNRAS, 500, 3064
Shetty, R., & Ostriker, E. C. 2006, ApJ, 647, 997
Simpson, R. J., Povich, M. S., Kendrew, S., et al. 2012, MNRAS, 424, 2442
Smith, R. J., Glover, S. C. O., Clark, P. C., Klessen, R. S., & Springel, V. 2014, MNRAS, 441, 1628
Smith, R. J., Treß, R. G., Sormani, M. C., et al. 2020, MNRAS, 492, 1594
Sormani, M. C., Sobacchi, E., Shore, S. N., Treß, R. G., & Klessen, R. S. 2017, MNRAS, 471, 2932
Sormani, M. C., Treß, R. G., Ridley, M., et al. 2018, MNRAS, 475, 2383
Soto, M., Barbá, R., Minniti, D., et al. 2019, MNRAS, 488, 2650
Urquhart, J. S., Figura, C., Cross, J. R., et al. 2021, MNRAS, 500, 3050
Wada, K., & Koda, J. 2004, MNRAS, 349, 270
Wang, K., Testi, L., Ginsburg, A., et al. 2015, MNRAS, 450, 4043
Ward-Thompson, D., Kirk, J. M., André, P., et al. 2010, A&A, 518, L92
Weaver, H. F. 1970, in Proceedings of the Sixth Symposium on Cosmical Gas Dynamics, Interstellar Gas Dynamics, 39, ed. H. J. Habing (Dordrecht: Reidel), 22
Zucker, C., Battersby, C., & Goodman, A. 2018, ApJ, 864, 153